analysis of spatial patterns in current species distributions could be a powerful approach for estimating levels of threat for the many regions and taxa with limited information on past distributions and landscape change, or with limited ecological information on species' habitat or climate associations. □

Methods

Distributions

British distribution sizes and fractal dimensions were calculated with the use of all records for each species in England, Wales and Scotland from 1970–82 (ref. 15) and 1995–99 (ref. 16). Occupied 10-km and 100-km squares were calculated with standard Ordnance Survey grid squares. Distribution maps were based on 65,826 species lists (that is, field visits) for 1970–82 (124,978 species × location distribution records), and 437,690 species lists for 1995–99 (1,548,935 records). Changes in distribution size were calculated by randomly resampling the 1995–99 species lists for each 100-km square to equalize recorder effort between the two periods[17]. Proportional change in distribution size was the number of 10-km squares occupied in 1970–82 subtracted from the number of squares occupied in the resampled 1995–99 data, divided by the number of squares occupied in 1970–82.

The analysis includes all resident butterfly species that have regularly been observed in Britain since 1970, apart from those species for which more than 40% of occupied grid squares in either period were migrants, vagrants or deliberate introductions[16]. Fifty-one species were included, none of which occupied 10% or more of their 100-km squares through migrants or introductions[16] (Supplementary Methods).

Area of occupancy and fractal dimension

Area of occupancy (in km^2) of each British species in each period was calculated at two scales, first by summing the areas of occupied 10-km squares, and second those of occupied 100-km squares. Log_{10}AOO at each scale was plotted against log_{10}(side of grid square (in km)), and the fractal dimension (D_{ij}) was the slope of this scale–area curve, subtracted from 2 (ref. 18). The fractal is used in these analyses as a descriptive measurement of spatial aggregation over a narrow range of scales: we do not imply that these species have 'truly' fractal distributions over multiple scales.

Estimating change

To estimate distribution change independently for each British species, 51 linear regressions of distribution change against D_{ij} and AOO (calculated at 10-km scale) were performed, leaving out each species in turn. Coefficients from the analysis with the remaining 50 species were used to estimate change with the use of D_{ij} and AOO for each omitted species. We tested the predictions by using a linear regression of observed change against estimated change for all 51 species (Fig. 2a, b).

Phylogenetic regression

The main results presented refer to linear regressions with species as independent data points, on the assumption that information on phylogenetic relatedness was not available (as might be typical for poorly recorded taxa). We tested the sensitivity of the results to phylogenetic relatedness with GLS regressions[29] implemented in the software package COMPARE[30] (Supplementary Methods). These analyses suggested that the evolutionary constraint acting on distribution pattern, size and change was small, and gave results consistent with those using species as independent data points. For analyses in which the proportion of variation explained is most important, R^2 from the phylogenetic GLS regression is presented alongside the raw results in the main text. Results from all other phylogenetic regressions are presented in Supplementary Information.

Flanders butterflies and British plants

Details of analyses are presented in Supplementary Methods.

Received 23 July; accepted 17 September 2004; doi:10.1038/nature03031.

1. Akçakaya, H. R. *et al.* Making consistent IUCN classifications under uncertainty. *Conserv. Biol.* **14,** 1001–1013 (2000).
2. Groombridge, B. & Jenkins, M. D. *World Atlas of Biodiversity* (Univ. California Press, Berkeley, CA, 2002).
3. Keith, D. A., Auld, T. D., Ooi, M. K. J. & Mackenzie, D. E. Sensitivity analyses of decision rules in World Conservation Union (IUCN) Red List criteria using Australian plants. *Biol. Conserv.* **94,** 311–319 (2000).
4. Mace, G. M. & Lande, R. Assessing extinction threats: towards a re-evaluation of IUCN threatened species categories. *Conserv. Biol.* **5,** 148–157 (1991).
5. World Conservation Monitoring Centre. *Global Biodiversity: Status of the Earth's Living Resources* (Chapman & Hall, London, 1992).
6. Hartley, S. & Kunin, W. E. Scale dependency of rarity, extinction risk, and conservation priority. *Conserv. Biol.* **17,** 1559–1570 (2003).
7. Warren, M. S., Barnett, L. K., Gibbons, D. W. & Avery, M. I. Assessing national conservation priorities: an improved red list of British butterflies. *Biol. Conserv.* **82,** 317–328 (1997).
8. World Conservation Union (IUCN). *IUCN Red List Categories. Version 3.1.* (World Conservation Union, Gland, Switzerland, 2001).
9. Cowley, M. J. R., Thomas, C. D., Thomas, J. A. & Warren, M. S. Flight areas of British butterflies: assessing species status and decline. *Proc. R. Soc. Lond. B* **266,** 1587–1592 (1999).
10. Johnson, C. N. Species extinction and the relationships between distribution and abundance. *Nature* **394,** 272–274 (1998).
11. Brown, J. H., Mehlman, D. W. & Stevens, G. C. Spatial variation in abundance. *Ecology* **76,** 2028–2043 (1995).
12. Rodríguez, A. & Delibes, M. Internal structure and patterns of contraction in the geographic range of the Iberian Lynx. *Ecography* **25,** 314–328 (2002).
13. Channell, R. & Lomolino, M. V. Dynamic biogeography and conservation of endangered species. *Nature* **403,** 84–86 (2000).
14. Shigesada, N. & Kawasaki, K. *Biological Invasions: Theory and Practice* (Oxford Univ. Press, Oxford, UK, 1997).
15. Heath, J., Pollard, E. & Thomas, J. A. *Atlas of Butterflies in Britain and Ireland* (Viking Books, Harmondsworth, UK, 1984).
16. Asher, J. *et al. The Millennium Atlas of Butterflies in Britain and Ireland* (Oxford Univ. Press, Oxford, UK, 2001).
17. Warren, M. S. *et al.* Rapid responses of British butterflies to opposing forces of climate and habitat change. *Nature* **414,** 65–69 (2001).
18. Kunin, W. E. Extrapolating species abundance across spatial scales. *Science* **281,** 1513–1515 (1998).
19. Ostling, A., Harte, J. & Green, J. L. Self-similarity and clustering in the spatial distribution of species. *Science* **290** (Suppl.), 671a (2000).
20. Condit, R. *et al.* Spatial patterns in the distribution of tropical tree species. *Science* **288,** 1414–1418 (2000).
21. Ripley, B. D. *Spatial Statistics* (John Wiley & Sons, New York, 1981).
22. Brooks, T. M., Pimm, S. L. & Oyugi, J. O. Time lag between deforestation and bird extinction in tropical forest fragments. *Conserv. Biol.* **13,** 1140–1150 (1999).
23. Hill, J. K., Thomas, C. D. & Huntley, B. Climate and habitat availability determine 20th century changes in a butterfly's range margins. *Proc. R. Soc. Lond. B* **266,** 1197–1206 (1999).
24. Hanski, I. *Metapopulation Ecology* (Oxford Univ. Press, Oxford, 1999).
25. Maes, D. & Van Dyck, H. Butterfly diversity loss in Flanders (north Belgium): Europe's worst case scenario? *Biol. Conserv.* **99,** 263–276 (2001).
26. Thomas, C. D. & Abery, J. C. G. Estimating rates of butterfly decline from distribution maps: the effect of scale. *Biol. Conserv.* **73,** 59–65 (1995).
27. Caughley, G. Directions in conservation biology. *J. Anim. Ecol.* **63,** 215–244 (1994).
28. Linder, E. T., Villard, M.-A., Maurer, B. A. & Schmidt, E. V. Geographic range structure in North American landbirds: variation with migratory strategy, trophic level, and breeding habitat. *Ecography* **23,** 678–686 (2000).
29. Martins, E. P. & Hansen, T. F. Phylogenies and the comparative method: a general approach to incorporating phylogenetic information into the analysis of interspecific data. *Am. Nat.* **149,** 646–667 (1997).
30. Martins, E. P. *COMPARE, version 4.6. Computer programs for the statistical analysis of comparative data* http://compare.bio.indiana.edu/ (Department of Biology, Indiana University, Bloomington IN, 2004).

Supplementary Information accompanies the paper on **www.nature.com/nature**.

Acknowledgements We thank the contributors to the butterfly and plant distribution surveys in Britain and Flanders; J. Asher and J. A. Thomas for calculating British rates of decline; and M. de la Cruz, A. Escudero, S. Hartley, J. Perry and M. Pocock for assistance with analyses. The work was supported by the UK Natural Environment Research Council. Maps were produced in DMap.

Competing interests statement The authors declare that they have no competing financial interests.

Correspondence and requests for materials should be addressed to R.J.W. (rwilson@escet.urjc.es).

Identification of human brain tumour initiating cells

Sheila K. Singh[1,2,3], Cynthia Hawkins[1,4], Ian D. Clarke[1,2], Jeremy A. Squire[6], Jane Bayani[6], Takuichiro Hide[1,2], R. Mark Henkelman[5], Michael D. Cusimano[3,7] & Peter B. Dirks[1,2,3]

[1]*The Arthur and Sonia Labatt Brain Tumor Research Centre,* [2]*Program in Developmental Biology,* [3]*Division of Neurosurgery,* [4]*Department of Pediatric Laboratory Medicine, and* [5]*Integrative Biology Program, The Hospital for Sick Children and University of Toronto, 555 University Avenue, Toronto, M5G 1X8, Canada*

[6]*Ontario Cancer Institute and University of Toronto, 610 University Avenue, Toronto, M5G 2M9, Canada*

[7]*Division of Neurosurgery, St Michael's Hospital and University of Toronto, 30 Bond Street, Toronto M5B 1W8, Canada*

The cancer stem cell (CSC) hypothesis suggests that neoplastic clones are maintained exclusively by a rare fraction of cells with stem cell properties[1,2]. Although the existence of CSCs in human leukaemia is established[3,4], little evidence exists for CSCs in solid tumours, except for breast cancer[5]. Recently, we prospectively isolated a $CD133^+$ cell subpopulation from human brain tumours that exhibited stem cell properties *in vitro*[6]. However,

the true measures of CSCs are their capacity for self renewal and exact recapitulation of the original tumour[1,2,7]. Here we report the development of a xenograft assay that identified human brain tumour initiating cells that initiate tumours *in vivo*. Only the CD133$^+$ brain tumour fraction contains cells that are capable of tumour initiation in NOD-SCID (non-obese diabetic, severe combined immunodeficient) mouse brains. Injection of as few as 100 CD133$^+$ cells produced a tumour that could be serially transplanted and was a phenocopy of the patient's original tumour, whereas injection of 10^5 CD133$^-$ cells engrafted but did not cause a tumour. Thus, the identification of brain tumour initiating cells provides insights into human brain tumour pathogenesis, giving strong support for the CSC hypothesis as the basis for many solid tumours[5], and establishes a previously unidentified cellular target for more effective cancer therapies.

Several studies have identified stem-like cells in brain tumour cultures[8–10]. By cell sorting for the cell surface antigen CD133 (refs 11–13), we demonstrated that a functional hierarchy exists in the brain tumour cell population *in vitro*[6]. To determine whether the CD133$^+$ human brain tumour cells were capable of tumour initiation *in vivo*, we compared the abilities of CD133$^+$ versus CD133$^-$ tumour cells to initiate tumour formation in NOD-SCID mouse brains. Immediately after surgical resection, solid, non-metastatic, brain tumour masses (medulloblastomas from three children, glioblastomas from three adults and one childhood glioblastoma; see Supplementary Table 1) were dissociated into single-cell suspensions. *In vitro* primary sphere formation assays were performed for all uncultured tumours and flow cytometric quantification of CD133 expression was performed on seven acutely dissociated tumours and two corresponding tumour xenografts before serial retransplantation. The CD133$^+$ fraction among highly aggressive glioblastomas (GBMs) ranged from 19 to 29%, and among medulloblastomas ranged from 6 to 21%, and correlated closely with an *in vitro* primary sphere formation assay (which we used to quantify stem cell frequency; see Supplementary Table 2). After dissociation, magnetic bead cell sorting was used to separate the CD133$^+$ brain tumour cells from their CD133$^-$ counterparts. Sorted cells were transplanted into the frontal lobe of six-week-old NOD-SCID mice.

Most intracranial xenograft models using human tumour cell lines or primary cultures require 10^5 to 10^6 cells for tumour engraftment and formation[14,15]. Analysis of mouse brains following CD133$^+$ engraftment revealed that as few as 100 CD133$^+$ cells were sufficient for the formation of human brain tumours in NOD-SCID mice that were analysed at 12–24 weeks post-injection (Fig. 1a–c) (see Supplementary Table 3). Injection of 50,000 to 100,000 of CD133$^-$ cells did not form tumours in the NOD-SCID brains, and histological examination at 12 weeks revealed only a glial scar tract from initial injection (Fig. 1d). A total of 15 CD133$^-$ injections and 19 CD133$^+$ injections were performed. Of the 19 mice injected with CD133$^+$ medulloblastoma or glioblastoma cells, 16 developed brain tumours (see Supplementary Table 3).

CD133$^+$ xenografts from two classic medulloblastomas showed small round blue cell morphology and demonstrated characteristic histologic structures (Homer–Wright rosettes)[16] (Fig. 2). CD133$^+$ xenografts from a third desmoplastic medulloblastoma recapitulated the more primitive cytoarchitecture associated with this subtype (Supplementary Fig. 1).

To further characterize the tumour phenotype of the CD133$^+$ medulloblastoma xenografts, we performed detailed immunohistochemical analyses of each transplanted tumour and of the original patients' tumours that were used for initial histologic diagnosis (see Supplementary Table 3). The CD133$^+$ xenografts from all three medulloblastomas expressed the cytoplasmic primitive intermediate filaments nestin[17](Fig. 2) and vimentin (data not shown), frequently used as neural precursor cell markers, although they are not definitive neural stem cell markers. All three medulloblastoma xenografts expressed the neuronal marker βIII-tubulin in a significant number of tumour cells, as did the original tumours from the patients (Fig. 2). Expression of the astrocyte marker GFAP (glial fibrillary acidic protein) was also seen in a minority of the human tumour cells in two of three medulloblastoma xenografts (Fig. 2). The GFAP-positive cells are morphologically neoplastic cells and did not demonstrate hybridization with mouse centromeric probes by interphase fluorescence *in situ* hybridization (FISH, data not shown) supporting that they were derived from the human cell transplant and were not trapped normal mouse astrocytes. Proliferative indices, indicated by MIB-1 (Ki67) immunostaining, were comparable in the xenografts and the original tumours (Fig. 2).

CD133$^+$ xenografts from the adult and childhood GBMs demonstrated classical histopathological features of this tumour type. Both the classical GBM and the diffusely infiltrative GBM (Fig. 3 and Supplementary Fig. 1) possessed the four diagnostic criteria as defined by the World Health Organization[18]. In each case, the phenotype of the mouse xenograft matched that of the patient's original tumour.

CD133$^+$ GBM xenograft phenotype was further studied by immunohistochemistry (Fig. 3). GBM xenografts also expressed nestin, showing a heterogeneous staining pattern that was consistent with the patients' original tumours. MIB-1 immunostaining showed a high degree of proliferation in both xenografts and the original tumours. CD133$^+$ GBM xenografts also demonstrated characteristic expression of GFAP resembling the original patients' tumours, but also showed immunostaining for the neuronal marker MAP2 (microtubule associated protein) in the human tumour cells, which did not label with mouse-specific centromeric probes by FISH (data not shown). This finding of the expression of markers for both neuronal and astrocyte lineages within the CD133$^+$ xenograft reflects an ability of the brain tumour initiating cells (BTIC) for multilineage, albeit cancerous, differentiation *in vivo*. In addition, immunostaining for p53 also revealed a similar increase in nuclear staining pattern for this tumour suppressor protein in the patient tumour and xenograft.

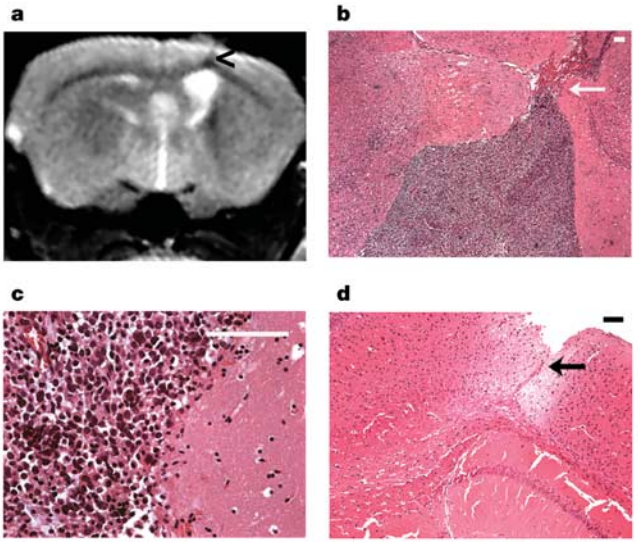

Figure 1 CD133$^+$ tumour cells initiate tumours upon intracranial transplantation into the adult NOD-SCID mouse forebrain. **a**, Magnetic resonance imaging (MRI) scan of a mouse injected with 1,000 CD133$^+$ medulloblastoma cells shows an enhancing mass under the injection tract (arrowheads) 14 weeks post-injection. **b**, **c**, Low (**b**) and high (**c**) magnification histological sections of the xenograft show a highly cellular mass below the injection site (white arrow in **b**). **d**, Histological section of mouse brain injected with CD133$^-$ medulloblastoma cells shows the injection tract (black arrow), but no tumour formation. Scale bar on all panels represents 100 microns.

CD133 immunostaining of the GBM xenografts revealed islands of positive cells, or single positive cells, amid large groups of negative cells; this indicates that not every cell in the xenograft is $CD133^+$ (Fig. 4a). Double immunostaining for CD133 and GFAP in $CD133^+$ xenografts from GBM samples demonstrated that these markers were expressed in different tumour cell subpopulations, suggesting that undifferentiated and differentiated tumour cells coexist within the transplanted tumours (Fig. 4b). A purified but small number of transplanted $CD133^+$ cells (Fig. 4c) resulted in a heterogeneous primary xenograft consisting of a minority of $CD133^+$ cells (19–22%) and a majority of $CD133^-$ cells (78–81%) (Fig. 4d). These results suggest that a tumour hierarchy exists in which the $CD133^+$ cells may generate $CD133^-$ tumour cells. These data are consistent with our previous observations, which demonstrate that only the $CD133^+$ fraction is proliferating and

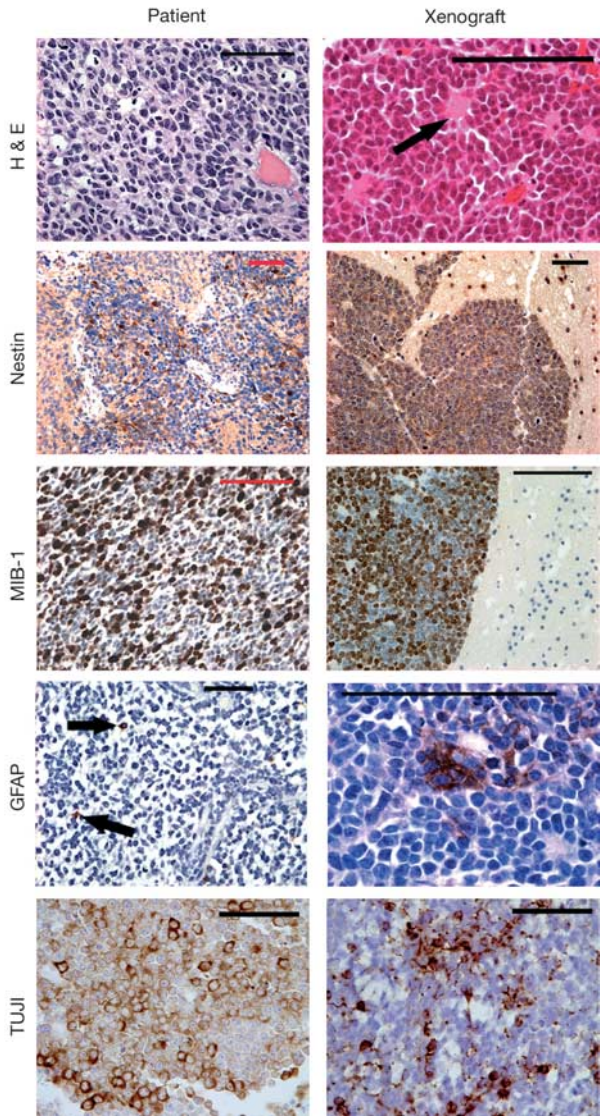

Figure 2 $CD133^+$ xenograft from a medulloblastoma (right side) resembles the original patient tumour (left side). H&E of a $CD133^+$ xenograft from patient 3 shows classical medulloblastoma cytoarchitecture, resembling the original patient's histology; a Homer–Wright rosette is indicated (arrow). The xenograft and the original tumour both express the neural precursor cell marker nestin (brown) and the neuronal marker βIII-tubulin (TUJI), and show a high proliferative index (MIB-1, brown nuclear staining), which is further increased in the xenograft. The astrocyte cell marker GFAP is also expressed in a small number of cells in the patient tumour and xenograft (brown, see arrows). Scale bar, 100 microns.

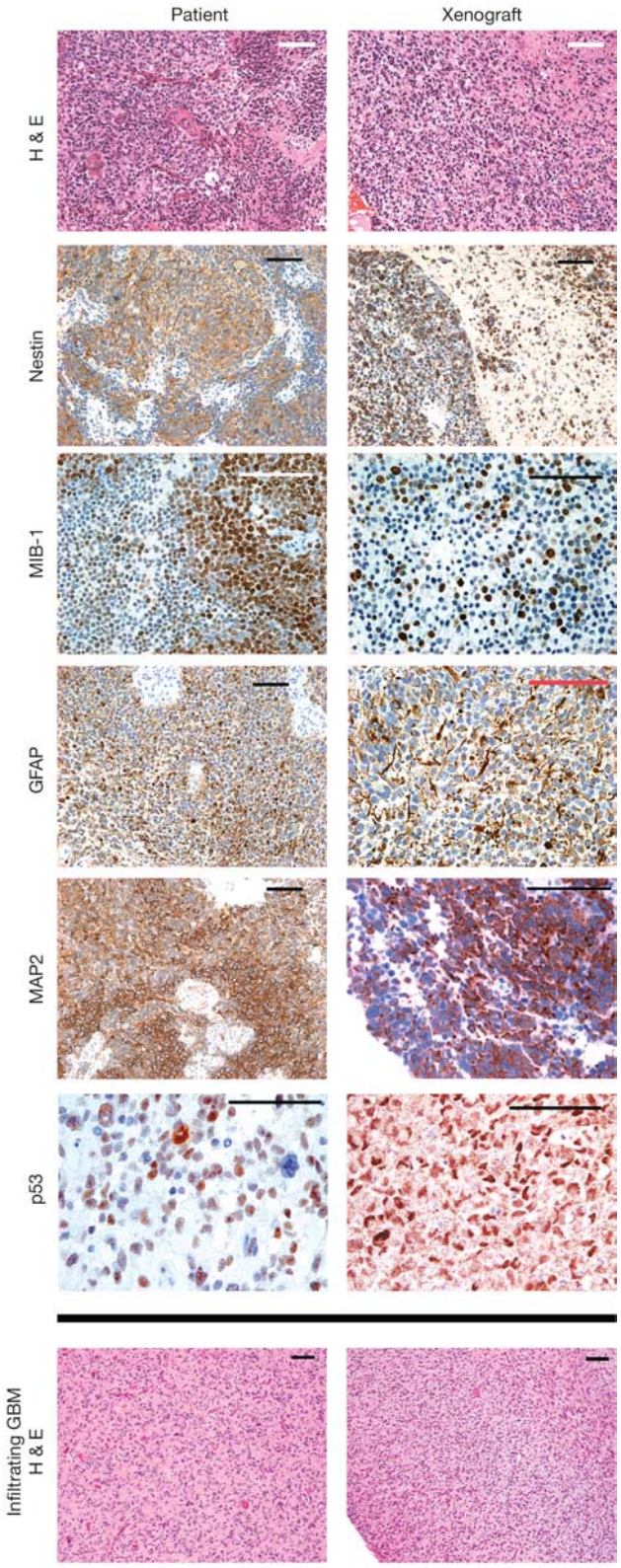

Figure 3 $CD133^+$ xenograft from a GBM (right) resembles the original patient tumour (left). H&E section of a $CD133^+$ xenograft from patient 5 shows histological features of a GBM, reflecting the patient's original tumour histology. Both the $CD133^+$ BTIC xenograft and the patient's original tumour show expression of the neural precursor marker nestin, high proliferative indices (MIB-1), p53 expression, and expression of both neuronal and astrocyte differentiated cell markers (MAP2 and GFAP). There are many invading human-specific nestin-positive tumour cells beyond the tumour borders in the xenograft. A diffusely infiltrative GBM (patient 7) is also depicted by H&E (bottom). Scale bar, 100 microns.

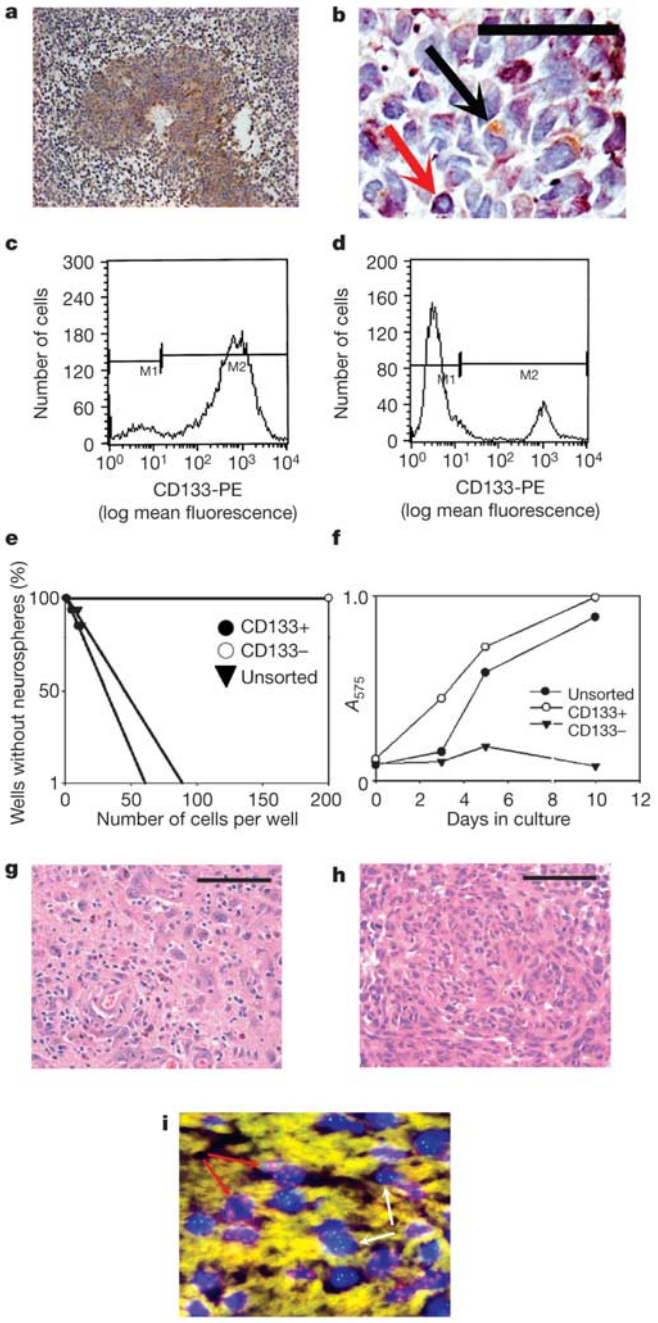

Figure 4 Only the CD133$^+$ BTIC, and not the CD133$^-$ tumour cell, is capable of tumour initiation. **a**, A subpopulation of cells from a CD133$^+$ GBM xenograft are CD133$^+$ (brown). **b**, Undifferentiated CD133$^+$ (brown, black arrow) and differentiated GFAP$^+$ (purple, red arrow) cells coexist in distinct subpopulations in this GBM xenotransplant. **c**, Purity of CD133$^+$ cells (84%) before initial xenotransplantation. M1, CD133$^-$ cells; M2, CD133$^+$ cells. **d**, Example of acutely dissociated primary xenotransplant; 19% CD133$^+$, 81% CD133$^-$. **e**, **f**, Limiting dilution analysis (**e**) and proliferation assays (**f**) of the GBM sorted for CD133 show that CD133$^+$ cells exclusively proliferate and self renew *in vitro*. Absorbance in **f** was measured at 575 nm. **g**, **h**, H&E sections of a recurrent paediatric GBM from the original patient (**g**, patient 6) and from a secondary xenograft from this tumour (**h**). **i**, Paraffin FISH of CD133$^-$ GBM xenograft shows that CD133$^-$ human tumour cells survive after xenotransplant but do not form tumours (human pan-centrometic probes in green, white arrows; mouse pan-centromeric probe in red, red arrows). Scale bar, 100 microns.

demonstrating self renewal *in vitro* (Fig. 4e, f).

A key property of all normal and cancer stem cells is the ability to self renew, a feature that can only be tested by serial passage. To determine whether the CD133$^+$ BTIC had self-renewal capacity, we performed serial retransplantation experiments from primary xenografts derived from a paediatric and an adult GBM (patients 6 and 7) that grew from an initial injection of 1,000 CD133$^+$ cells. After 6 weeks, the primary tumour was excised from the mouse brain and 1,000 CD133$^+$ cells were isolated and then reinjected into secondary mice. After 5 weeks, we observed that two out of two secondarily xenografted mice from the paediatric GBM and three of three mice from the adult GBM had brain tumours that recapitulated the phenotype of the original patient tumour and the primary xenograft (Fig. 4g, h), providing direct evidence for the self-renewal capacity of this population.

Most notably, none of the mice injected with CD133$^-$ tumour cells, purified to near homogeneity, developed brain tumours when analysed at 12 weeks post-injection. On the basis of analysis of flow histograms of tumour cells sorted for CD133, the contaminating CD133$^+$ cells in the purified CD133$^-$ population represent a weakly staining population that has very low CD133 protein expression, rather than the highly staining true CD133$^+$ sorted population (see Methods). To determine whether viable CD133$^-$ human cells had engrafted into the mouse brain but did not form tumours, we performed interphase FISH analysis of murine brain sections using species-specific centromeric probes to detect the presence of human cells at the injection site (Fig. 4i). For each of the CD133$^-$ injections from five medulloblastoma and glioblastoma human brain tumour samples (patients 1–5), human cells could be found in small clusters near the original injection site, but these cells did not form a nodule or mass; this indicates that their inability to form tumours is cell intrinsic, and not owing to an inability to be adequately supported in the brain environment following transplant.

To demonstrate that all engrafted cells have undergone a transformation event and do not represent normal brain cells, we conducted molecular cytogenetic analysis by spectral karyotyping (SKY) and interphase FISH using preparations obtained directly from briefly cultured tumour cells sorted for CD133. We found that both CD133$^-$ and CD133$^+$ tumour cells from a medulloblastoma exhibited chromosomal instability for chromosome 17. The normal signal pattern of two centromere signals and two TP53 signals was detected in less than 4% of sorted cells that were subsequently xenotransplanted, indicating a low rate of potential normal cell contamination (see Supplementary Fig. 2). SKY analysis of GBM specimens bore chromosomal aberrations characteristic of this tumour type (see Supplementary Fig. 3). Further interphase FISH analysis of this GBM using centromere 7 indicated that nearly 80% of both CD133$^+$ and CD133$^-$ cells exhibited an abnormal karyotype, consistent with the SKY findings. Paraffin FISH studies performed on CD133$^+$ xenografts from an adult GBM also indicated that the majority of cells bore evidence of transformation, with amplification of the EGFR gene identical to that of the patient's tumour (see Supplementary Fig. 4). These cytogenetic data indicate that the transplanted cells, whether CD133$^-$ or CD133$^+$, have an abnormal karyotype and aneusomy pattern inconsistent with significant contamination by normal cells. The CD133$^+$ and CD133$^-$ cells have the same cytogenetic alterations, suggesting that they are clonally derived.

Together, these data indicate that the CD133$^+$ human brain tumour cell fraction from tumours of different types, from both adults and children, contain brain tumour initiating cells that exclusively initiate tumour formation in immunodeficient mice. BTIC have potent *in vivo* self-renewal and proliferative capacities, generating tumours that are a phenocopy of the patient's tumour following engraftment with as few as 100 CD133$^+$ cells. Thus, the BTIC possess all the key properties ascribed to a stem cell. These results indicate that brain cancer should not be viewed as blocked or

frozen differentiation; rather, the brain tumour initiating cell clone exhibits patterns of abnormal differentiation. Although our model demonstrates that tumours are initiated by $CD133^+$ cells with stem cell properties, whether the cancer-initiating event occurs in a normal stem cell or in normal progenitor or differentiated cells that have reacquired stem cell properties remains to be determined.

Although the frequency of cancer-initiating cells in brain tumours is higher than reported for other cancers[4,5], we suggest that the cancer-initiating frequency may be higher because these tumours are among the most aggressive known human cancers and our patient samples were also derived from within the patient's untreated primary tumour masses. Further *in vivo* limiting dilution analysis will continue to more accurately determine the CSC frequency within the $CD133^+$ population.

These results suggest that brain cancers are hierarchically organized and lend strong support for the CSC hypothesis, extending this idea beyond the original studies on human leukaemias[3,4,7,19]. The CSC hierarchy may be functionally elucidated as more surface markers for neural stem cells emerge, and more potent stem cell activity may be found in a $CD133^+$ subpopulation. Leukaemias have been suggested to originate in stem cell[4] as well as progenitor populations[20,21], and the question of cell of origin remains unclear in brain tumours[22–25].

The identification of an *in vivo* tumour-initiating cell from human brain tumours of different phenotypes provides a powerful tool to investigate the tumorigenic process in the central nervous system. We have also efficiently created a model that can be used to study each individual patient's brain tumour. The cellular heterogeneity of brain tumours dictates that if only a small fraction of cancer stem cells is capable of regenerating the tumour, bulk therapy may fail to target the tumour-initiating cell, allowing for disease progression or relapse. The functional analysis of the BTIC may give new insight into patient prognosis that may then warrant individual tailoring of therapy.

Note added in proof: While our manuscript was under consideration, Galli *et al.*[28] demonstrated that glioblastoma cell lines, established by culture in neurosphere conditions, could proliferate, self renew and differentiate into multiple lineages *in vitro*. Cerebral injection of 200,000 of these tumour sphere cells could also generate tumours *in vivo*, and after repeat culture, could initiate phenotypically similar tumours, in a secondary mouse. □

Methods

Primary tumour sphere culture

Tumour samples were obtained from consenting patients, as approved by the Research Ethics Boards at The Hospital for Sick Children and St Michael's Hospital (Toronto). Tumours were washed, acutely dissociated in oxygenated artificial cerebrospinal fluid (CSF) and subject to enzymatic dissociation. Tumour cells were then briefly placed in tumour sphere media (TSM) to allow for recovery following enzymatic dissociation[6]. On average, each tumour specimen yielded two to five million cells.

Magnetic cell sorting and flow cytometry

Cells were labelled with 1 μL CD133/1 microbeads per 1 million cells using the Miltenyi Biotec CD133 cell isolation kit, as previously described[6], between 1–24 h post-dissociation (median 2.75 h). Tumour cells were generally very adherent and required frequent mechanical and chemical trituration to prevent cell clumping during sorting. Aliquots of $CD133^+$ and $CD133^-$ sorted cells were evaluated for purity by flow cytometry with a FACSCalibur machine (BD Biosciences), using CD133/2 (293C3)-PE antibody (Miltenyi Biotec). Purities ranged from 70 to 91% for $CD133^+$ cells (median 84%), and 87.5 to 99.5% (median 99.5%) for $CD133^-$ cells. The small impurity of $CD133^+$ cells in the $CD133^-$ fraction quantified by FACS showed very low mean fluorescence in comparison to sorted $CD133^+$ cells, which had high fluorescence; this suggests that these contaminating $CD133^+$ cells in the $CD133^-$ fraction are phenotypically different from the sorted $CD133^+$ population that were used in our transplantation studies.

Intracranial cell transplantation into NOD-SCID mice

Within 1 to 16 h of magnetic bead cell sorting, purified populations of $CD133^+$ and $CD133^-$ cells were resuspended in 10 μl of phosphate buffered saline (PBS), in aliquots of 50,000, 10,000, 5,000 and 1,000 $CD133^+$ cells (as few as 100 $CD133^+$ cells were used for patients 6 and 7) and 50,000 or 100,000 $CD133^-$ cells. These aliquots were injected stereotactically into 6- to 8-week-old NOD-SCID mouse frontal cortex, following administration of general anaesthesia. The injection coordinates were 3 mm to the right of the midline, 2 mm anterior to the coronal suture and 3 mm deep.

Mouse brain fixation and histopathology

Mice were killed and their brains were immediately removed and fixed in 4% paraformaldehyde for 24 h, then transferred to 70% ethanol. Mouse brains were processed on a Tissue-Tek VIP (Sakura) and embedded in paraffin. Brains were sectioned at 5-μm thickness on a Microm HM 200 cryotome (Eryostar), and stained with haematoxylin-and-eosin (H&E) as per standard histopathological technique.

Immunohistochemistry

Paraffin embedded, 5-μm formalin fixed tissue sections were mounted on microscope slides. Tissue sections were then dried overnight at 60 °C, dewaxed in xylene and rehydrated with distilled water. With the exception of sections stained for GFAP, all sections were treated with heat-induced epitope retrieval technique (HIER) using a citrate buffer at pH 6.0. Incubation with the following antibodies was performed for 1 h at room temperature: βIII-tubulin (Chemicon, 1:500), GFAP (DakoCytomation, 1:1,000), MIB-1 (DakoCytomation, 1:20) nestin (Chemicon, 1:200), MAP2 (Sigma, 1:1,000) and p53 (DAKO, 1:20). Immunostaining was performed on a Ventana NEXES auto-immunostainer (Ventana Medical Systems). Double immunostaining for CD133 and GFAP used anti-human CD133 (Miltenyi Biotec, 1:5) incubated overnight at room temperature, followed by anti-human GFAP (DAKO, 1:1,000) for 1 h at room temperature. Human placenta[11,26] and human retinoblastoma specimens were used as positive controls for CD133. Immunodetection was performed using the Elite Vector Stain ABC System (Vector Laboratories). The counterstain of preference was haematoxylin for nuclear detail.

In vitro limiting dilution analysis (primary sphere formation assays)

Limiting dilution assay on tumour cells that had been sorted for CD133 was performed and 0.37 intercepts calculated[6]. Primary sphere formation assays were performed on the entire acutely dissociated tumour cell population on day 0 to quantify stem cell frequency within the tumour, as previously described[6]. Cell proliferation assays were performed on days 0, 3, 5 and 7 post-plating using the Roche MTT-based colorimetric assay cell proliferation kit 1. Cells were plated in 96-well microwell plates in 0.1-ml volumes of TSM, at a density of 1,000 cells per well.

Cytogenetic preparation, FISH analysis and spectral karyotyping of tumour sphere cells

Short-term cultured sorted or unsorted cells were colcemid treated, hypotonically swelled and methanol:acetic acid treated as previously described[27]. Interphase FISH analysis was performed using commercially available probes for centromere 17 and the locus specific probe for p53, as well as the centromere 7 and EGFR probe set (Vysis), and used according to the manufacturer's instructions. Pancentromeric mouse and human specific probes (Cedarlane) were also used. The slides were visualized and imaged using the Quips Imaging System (Vysis). Two-hundred nuclei were scored for each cell population and tabulated. Spectral karyotyping was performed on metaphase spreads using the commercially available probes supplied by Applied Spectral Imaging, and analysed as previously described[27].

Received 7 September; accepted 22 October 2004; doi:10.1038/nature03128.

1. Reya, T., Morrison, S. J., Clarke, M. F. & Weissman, I. L. Stem cells, cancer, and cancer stem cells. *Nature* **414,** 105–111 (2001).
2. Pardal, R., Clarke, M. & Morrison, S. Applying the principles of stem-cell biology to cancer. *Nat. Rev. Cancer* **3,** 895–902 (2003).
3. Lapidot, T. *et al.* A cell initiating human acute myeloid leukaemia after transplantation into SCID mice. *Nature* **367,** 645–648 (1994).
4. Bonnet, D. & Dick, J. E. Human acute myeloid leukemia is organized as a hierarchy that originates from a primitive hematopoietic cell. *Nature Med.* **3,** 730–737 (1997).
5. Al-Hajj, M., Wicha, M. S., Benito-Hernandez, A., Morrison, S. J. & Clarke, M. F. Prospective identification of tumorigenic breast cancer cells. *Proc. Natl Acad. Sci. USA* **100,** 3983–3988 (2003).
6. Singh, S. K. *et al.* Identification of a cancer stem cell in human brain tumors. *Cancer Res.* **63,** 5821–5828 (2003).
7. Dick, J. E. Breast cancer stem cells revealed. *Proc. Natl Acad. Sci. USA* **100,** 3547–3549 (2003).
8. Ignatova, T. N. *et al.* Human cortical glial tumors contain neural stem-like cells expressing astroglial and neuronal markers *in vitro*. *Glia* **39,** 193–206 (2002).
9. Hemmati, H. D. *et al.* Cancerous stem cells can arise from pediatric brain tumors. *Proc. Natl Acad. Sci. USA* **100,** 15178–15183 (2003).
10. Kondo, T., Setoguchi, T. & Taga, T. Persistence of a small subpopulation of cancer stem-like cells in the C6 glioma cell line. *Proc. Natl Acad. Sci. USA* **101,** 781–786 (2004).
11. Miraglia, S. *et al.* A novel five-transmembrane hematopoietic stem cell antigen: isolation, characterization, and molecular cloning. *Blood* **90,** 5013–5021 (1997).
12. Corbeil, D., Roper, K., Weigmann, A. & Huttner, W. B. AC133 hematopoietic stem cell antigen: human homologue of mouse kidney prominin or distinct member of a novel protein family? *Blood* **91,** 2625–2626 (1998).
13. Uchida, N. *et al.* Direct isolation of human central nervous system stem cells. *Proc. Natl Acad. Sci. USA* **97,** 14720–14725 (2000).
14. Houchens, D. P., Ovejera, A. A., Riblet, S. M. & Slagel, D. E. Human brain tumor xenografts in nude mice as a chemotherapy model. *Eur. J. Cancer Clin. Oncol.* **19,** 799–805 (1983).
15. Hu, B. *et al.* Angiopoietin-2 induces human glioma invasion through the activation of matrix metalloprotease-2. *Proc. Natl Acad. Sci. USA* **100,** 8904–8909 (2003).
16. Russell, D. & Rubenstein, L. *Pathology of Tumors of the Central Nervous System* (Williams and Wilkins, Baltimore, 1989).

17. Lendahl, U., Zimmerman, L. B. & McKay, R. D. CNS stem cells express a new class of intermediate filament protein. *Cell* **60,** 585–595 (1990).
18. Kleihues, P. *et al.* The WHO classification of tumors of the nervous system. *J. Neuropathol. Exp. Neurol.* **61,** 215–225; discussion 226–229 (2002).
19. Hope, K. J., Jin, L. & Dick, J. E. Acute myeloid leukemia originates from a hierarchy of leukemic stem cell classes that differ in self-renewal capacity. *Nature Immunol.* **5,** 738–743 (2004).
20. Cozzio, A. *et al.* Similar MLL-associated leukemias arising from self-renewing stem cells and short-lived myeloid progenitors. *Genes Dev.* **17,** 3029–3035 (2003).
21. Passegue, E., Jamieson, C. H., Ailles, L. E. & Weissman, I. L. Normal and leukemic hematopoiesis: are leukemias a stem cell disorder or a reacquisition of stem cell characteristics? *Proc. Natl Acad. Sci. USA* **100**(suppl. 1), 11842–11849 (2003).
22. Holland, E. C., Hively, W. P., DePinho, R. A. & Varmus, H. E. A constitutively active epidermal growth factor receptor cooperates with disruption of G1 cell-cycle arrest pathways to induce glioma-like lesions in mice. *Genes Dev.* **12,** 3675–3685 (1998).
23. Holland, E. C. Gliomagenesis: genetic alterations and mouse models. *Nature Rev. Genet.* **2,** 120–129 (2001).
24. Bachoo, R. M. *et al.* Epidermal growth factor receptor and Ink4a/Arf: convergent mechanisms governing terminal differentiation and transformation along the neural stem cell to astrocyte axis. *Cancer Cell* **1,** 269–277 (2002).
25. Oliver, T. G. & Wechsler-Reya, R. J. Getting at the root and stem of brain tumors. *Neuron* **42,** 885–888 (2004).
26. Potgens, A. J., Bolte, M., Huppertz, B., Kaufmann, P. & Frank, H. G. Human trophoblast contains an intracellular protein reactive with an antibody against CD133–a novel marker for trophoblast. *Placenta* **22,** 639–645 (2001).
27. Bayani, J. *et al.* Molecular cytogenetic analysis of medulloblastomas and supratentorial primitive neuroectodermal tumors by using conventional banding, comparative genomic hybridization, and spectral karyotyping. *J. Neurosurg.* **93,** 437–448 (2000).
28. Galli, R. *et al.* Isolation and characterization of tumorigenic, stem-like neural precursors from human glioblastoma. *Cancer Res.* **64,** 7011–7021 (2004).

Supplementary Information accompanies the paper on **www.nature.com/nature**.

Acknowledgements We thank M. Borden, J. Ma, I. Diplock, M. Ho and C. Gibson for technical assistance, and we are grateful to V. Bonn, L. Davidson, N. Lifshitz and J. Chen of the Mouse Imaging Centre for help with neuroimaging. We thank J. Dick for discussions. S. Singh was supported by a a Terry Fox Foundation fellowship from the Canadian Cancer Society, the Neurosurgical Research and Education Foundation and the American Brain Tumor Association. This work was supported by the Canadian Cancer Society, the Canadian Institutes of Health Research, the Foundation of The Hospital for Sick Children, BrainChild and the Jack Baker and Jessica Durigon family funds.

Competing interests statement The authors declare that they have no competing financial interests.

Correspondence and requests for materials should be addressed to P.D. (peter.dirks@sickkids.ca).

A FADD-dependent innate immune mechanism in mammalian cells

Siddharth Balachandran*, Emmanuel Thomas* & Glen N. Barber

Department of Microbiology and Immunology and Sylvester Comprehensive Cancer Center, University of Miami School of Medicine, Miami, Florida 33136, USA

* These authors contributed equally to this work

Vertebrate innate immunity provides a first line of defence against pathogens such as viruses and bacteria. Viral infection activates a potent innate immune response, which can be triggered by double-stranded (ds)RNA produced during viral replication[1–3]. Here, we report that mammalian cells lacking the death-domain-containing protein FADD[4,5] are defective in intracellular dsRNA-activated gene expression, including production of type I (α/β) interferons, and are thus very susceptible to viral infection. The signalling pathway incorporating FADD is largely independent of Toll-like receptor 3 and the dsRNA-dependent kinase PKR, but seems to require receptor interacting protein 1 as well as Tank-binding kinase 1-mediated activation of the transcription factor IRF-3. The requirement for FADD in mammalian host defence is evocative of innate immune signalling in *Drosophila*, in which a FADD-dependent pathway responds to bacterial infection by activating the transcription of antimicrobial genes[6]. These data therefore suggest the existence of a conserved pathogen recognition pathway in mammalian cells that is essential for the optimal induction of type I interferons and other genes important for host defence.

A major consequence of virus infection is the induction of the type I interferons (IFNs), which are a family of cytokines essential for host defence[3,7]. While investigating the mechanisms of IFN antiviral activity, we noticed that early passage murine embryonic fibroblasts (MEFs) lacking the apoptosis adaptor molecule FADD appeared to be overtly sensitive to virus infection[8]. To examine this phenotype further, we infected $Fadd^{+/-}$ and $Fadd^{-/-}$ MEFs with the IFN-sensitive prototypic rhabdovirus vesicular stomatitis virus (VSV), and observed that VSV replication was markedly increased (>100-fold) in the $Fadd^{-/-}$ MEFs compared with their wild-type counterparts (Fig. 1a–c). Moreover, whereas pre-treatment with type I (α/β) or type II (γ) IFN for 12 h was seen to exert significant antiviral activity in normal cells, these key antiviral cytokines only delayed the onset of viral replication in $Fadd^{-/-}$ MEFs for 24–36 h, whereupon virus replication proceeded unchecked (Fig. 1a–c). The observed susceptibility to infection did not appear to be restricted to VSV, because MEFs lacking FADD were also sensitive to infection by other viruses, including influenza virus and encephalomyocarditis (EMCV) virus (Supplementary Fig. 1). MEFs lacking caspase 8 (refs 9, 10) (or cells treated with caspase inhibitors) exhibited no increased susceptibility to VSV infection compared to control cells, and retained the ability to be protected by IFN, suggesting that FADD exerts its antiviral effects independently of caspase 8 (Supplementary Fig. 2 and data not shown).

Because exposure to type I and II IFNs was unable to effectively protect $Fadd^{-/-}$ MEFs from virus replication, it is plausible that effective IFN-mediated, janus kinase (JAK)-activated STAT (signal transducer and activator of transcription) signalling[11] may require FADD. However, neither nuclear translocation of STAT1 nor the induction of selected type I and II IFN-responsive genes appeared to be impaired in $Fadd^{-/-}$ cells, indicating that IFN signalling *per se* is probably not compromised (Fig. 1d; see also Supplementary Fig. 3).

Despite these observations, it remained possible that the antiviral state initially established by 12 h of pre-exposure to exogenous IFN is short-lived and may require constant *de novo* synthesis of type I IFNs after virus infection (Fig. 1a). Indeed, we noted that continuous supplementation of recombinant type I IFNs to $Fadd^{-/-}$ cells after VSV infection conferred some protection against viral replication and cytolysis (Fig. 1e, f). The continual requirement for IFN induction after virus infection was further emphasized by demonstrating that antibody-mediated neutralization of secreted IFN-α or -β after exposure to VSV rendered normal cells susceptible to infection even after IFN pre-treatment (Fig. 1g, h).

These analyses suggest that an actual defect in the production of type I IFNs after virus/dsRNA detection might be responsible for the susceptibility of $Fadd^{-/-}$ cells to infection. To examine this possibility, we transfected $Fadd^{+/-}$ and $Fadd^{-/-}$ cells with a luciferase reporter construct under control of the IFN-β promoter and subsequently administered poly(I:C), a synthetic mimetic of viral dsRNA thought to be the primary trigger of IFN production after virus infection[3]. Notably, we found that transfected poly(I:C) triggered robust (~10-fold) induction of the IFN-β promoter in $Fadd^{+/-}$ cells but not in $Fadd^{-/-}$ cells (Fig. 2a). The induction of the IFN-β promoter was not observed using non-transfected, exogenous poly(I:C) alone (Fig. 2a). Poly(I:C)-induced activation of IFN-β promoter-driven luciferase activity could be partially restored by reintroducing murine FADD into $Fadd^{-/-}$ MEFs (Supplementary Fig. 4). A requirement for FADD in dsRNA-induced activation of the IFN-β promoter was further confirmed by short interfering RNA (siRNA)-mediated suppression of FADD in HeLa cells (Supplementary Fig. 4).